

An Experimental Investigation of the Effect of Aspect Ratio on the Airfoil Characteristics of NACA 0012 Wing

Mahbubur Rahman^{1*}, Mohammad Ali², Md. Mostofa Hossain³

^{1, 2}Department of Mechanical Engineering, Bangladesh University of Engineering & Technology, Bangladesh

³Department of Mechanical Engineering, Sonargaon University, Bangladesh

***Corresponding Author**

E-mail Id:-mahbubmithu75@gmail.com

ABSTRACT

The aspect ratio has a great effect on the aerodynamic characteristics. It is an important technique for the improvement of aerodynamic performance through drag reduction. The effect of aspect ratio on the airfoil performance is investigated about axially symmetric wings as a function of the angle of attack. Optimum design of lifting surface provides maximum possible lift force and minimum possible drag force. The wind tunnel used for the experiments is an open conduit and has a 1200x1200 mm² x-section with a closed test chamber. Three different types of airfoil with different aspect ratios (AR 2, AR 1, and AR 0.5) are tested under the airflow speed of 37.5m/s. It is found that for the same wing area wing model of AR 2 reduces the strength of the vortices at the wingtip by reducing the tip vortex more effectively than any other wing models and as a result, the difference between the upper and lower surface pressures on wing model of AR 2 is comparatively higher than that of other wing models at various angles of attack. After analyzing the results, the wing model AR 2 is found to be the optimum.

Keywords:-Airfoil, Aspect ratio, Angle of attack, Lift force, Drag force, Symmetric wing, Wind tunnel.

INTRODUCTION

A force is exerted on the surface of a body when a fluid past over it. The perpendicular component to the flow direction of that force is called lift. On the other hand, parallel component of that force to the flow direction is called drag force. Wings is the most ordinary element that is related to lift. Various factors affect lift force most importantly the shape of the aero-foil and the amount of camber. However, flow separation limits the maximum lift at a rated speed. Makwana et al. [1] did numerical solution of flow over airfoil where they focused on different technique to reduce flow separation and also gave some idea about different model of CFD. They concluded that to improve the performance of airfoil either lift

coefficient must be increased or drag should be decreased and pressure coefficient must be properly distributed on the airfoil surface. The development of wing theory led to the concept of wing-section characteristics that were derived from data obtained from tests of finite-aspect-ratio wings, which were then used to predict the characteristics of wings of different plan forms [5]. Martinat et al. [6] studied the NACA0012 dynamic stall at Reynolds numbers 10^5 and 10^6 by means of two- dimensional and three-dimensional numerical simulations. The result has shown that the downstroke phases of the pitching motion are subjected to strong three-dimensional turbulence effects along the span, whereas the flow is practically two-

dimensional during the upstroke motion. Aşkan et al. [7] investigated the impact of aspect ratio on the aerodynamic performances and flow separation behavior on a model wing made up four different profiles used to the wing of the Boeing 737-Classic aircrafts. They observed from the experiments and numerical studies that the changing of the aspect ratio affected the drag as well as lift and also flow separation. They concluded that the increases in aspect ratio and in angle of attack have been triggered flow separation. Several experiments have been carried out both numerical and experimental to find out the optimum design of the airfoil for maximum lift and minimum drag. An experimental investigation is carried out in the wind tunnel to find the aerodynamic performance of curved-edge planform of NACA 4412 airfoil by Nazmul et al.[8]. After analyzing Coefficient of Lift, Coefficient of Drag and Lift to Drag ratio of different wing models from the static pressure distribution, they found that the curved leading-edge wing planform had larger lift coefficient and lower drag coefficient than the rectangular planform. The results showed that, the curved trailing edge planform had higher lift coefficient and lower drag coefficient than the curved leading-edge wing. From the experimental results, it is also found that among the three types of planforms the curved trailing edge wing planform had the largest lift to drag ratio. They concluded that due to reduction in the chord length near the tip of the curved-edge wings, the tip loss was also reduced and for that the aerodynamic performance of the curved edge planforms were found better than that of the rectangular platform. interference effect occurs in between the aero foils of biplane configurations. It varies with the change of angle of attack and chord length. Ala [9] analyzed the interference effect of different biplane configurations of NACA 0024 symmetric aero foil with chord length of 100mm for four biplane

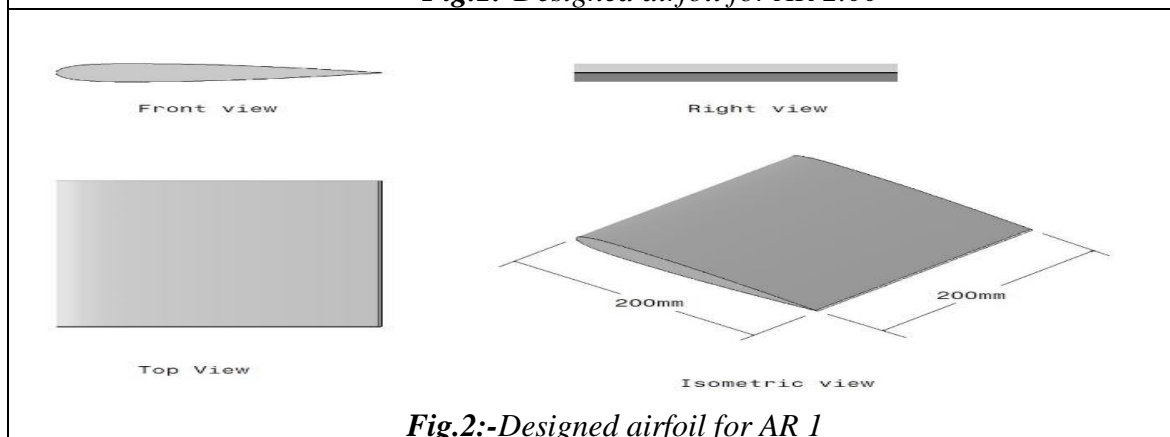
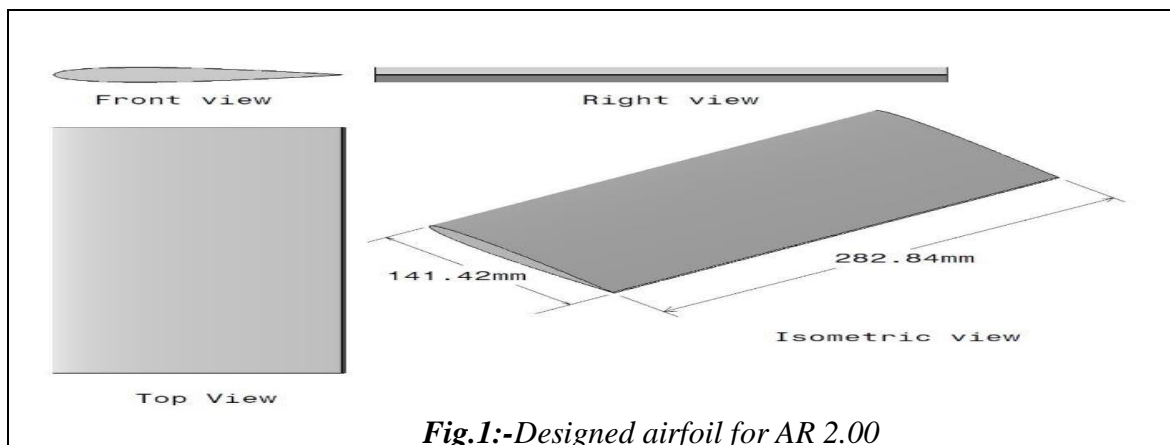
configurations. The numerical results showed that for biplane configurations of NACA 0024 profile, the computational value of lift coefficient is maximum at 18° angle of attack for 0.40, 0.50 and 0.75 of chord length while for the biplane at 1.00 of chord length, the maximum value is observed approximately at 21° angle of attack. The effect of the aspect ratio on the aerodynamic characteristics of rectangular wings was experimentally investigated at low Reynolds numbers by Mizoguchi et al. [10] where aspect ratio was considered to be caused by wingtip vortices, the effects of the Reynolds number, the shape of the leading edge, and the thickness ratio. Kopac et al. 2005 [11] investigated the effect of aspect ratio on the airfoil performance for airfoil about axially symmetric wings as function of angle of attack. From the analysis of the incompressible viscous flow fields different type of wing models were experimented by TE54 wind tunnel which had a 300×300 mm x-section under the airflow speed of 33.76 m/s. Experimental results showed that wing model having higher aspect ratio yields the optimum performance. Shehata et al. 2017 [12] revealed that the pressure distribution over an airfoil surface is influenced by suction slot and it have a significant effect on lift and drag coefficients. Ara et al. [13] studied the aerodynamic performance of winglets with curved edge wing of NACA 4412 where they found that for wing models with winglets lift to drag ratios increased and induced drag decreased compared to wing models without winglet. They concluded that less wing tip vortices are generated on the tip of the wing for higher aspect ratio and aspect ratio of the wing significantly responsible for the performance lift and drag. CFD analysis of the flow over NACA 0012 airfoil had been done by Patel et al. [14] where they concluded that at the zero degree of AOA there is no lift force generated and to increase amount of lift force and value of

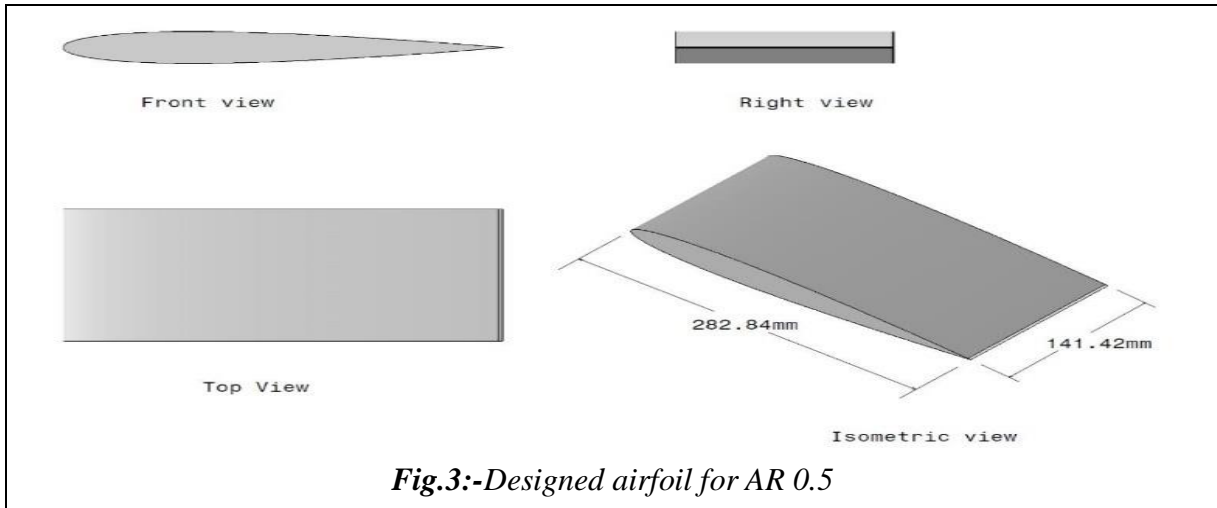
lift coefficient, the value of AOA must be increased. An analysis of pressure coefficient of NACA 4412 airfoil at AOA ranging from 0° to 12° using CFD was done by Kevadiya [15] where the results showed that with the increase of AOA, the pressure coefficient on the upper surface decreased and lower surface increased. As the efficiency of the aircraft greatly depends on the size and shape of the wing, several researches are still carried out throughout the world to find maximum possible lift and minimum possible drag. For this, an effort has been taken to investigate the effect of aspect ratio on the Airfoil characteristics of NACA 0012 wing through experiment by using wind-tunnel.

MODEL CONSTRUCTION

The three-chord length of the models are 141.42 mm, 200mm and 282.84mm with span of 282.84mm, 200mm and 141.42mm respectively. The wing models are

manufactured with extreme precision for taking data. To obtain that objective wing models of different aspect ratios (AR 0.5, AR 1, AR 2) are designed in Solid Works having the equal surface area of 40000 mm² as shown in Figure 1,2 and 3 respectively. Then the airfoil shapes are cut to get precise size and shape. From those drawings wing models are made by wood. Also, appropriate fixture is made to set the models in the wind tunnel and a multi-tube manometer is fabricated to take the pressure readings from the surfaces of the wing models. Each model is provided with 32 pressure tapings along the span and chord (16 at upper surface and 16 at lower surface). The wing models are divided into four equal segments (A, B, C and D) along the span. Four pressure tapping points at upper surface and four pressure tapping points at lower surface are made at 20%, 40%, 60% and 80% of the average chord length of each segment of all the wing models.





MATHEMATICAL MODELING

The wind tunnel has a reference pressure tap located upstream of the test section and the pressure there is:

$$P_{\infty} = p_{water} g (h_{atm} - h_{\infty}) \quad (1)$$

From the Bernoulli relation, the corresponding velocity along a horizontal streamline is:

$$V_{\infty} = \sqrt{\frac{2p_{water} g (h_{atm} - h_{\infty})}{p_{air}}} \quad (2)$$

The pressure taps provide pressure values determined from the manometer

as:

$$P_i = p_{water} g (h_{atm} - h_i) \quad (3)$$

Figure 4 [6,7] shows the pressure distribution at any point over the surface in terms of the pressure coefficient C_p , which is defined as follows:

$$C_p = \frac{P_{Local} - P_{\infty}}{\frac{1}{2} \rho V_{\infty}^2} \quad (4)$$

Where, $\frac{1}{2} \rho V_{\infty}^2$ is the free stream dynamic pressure head

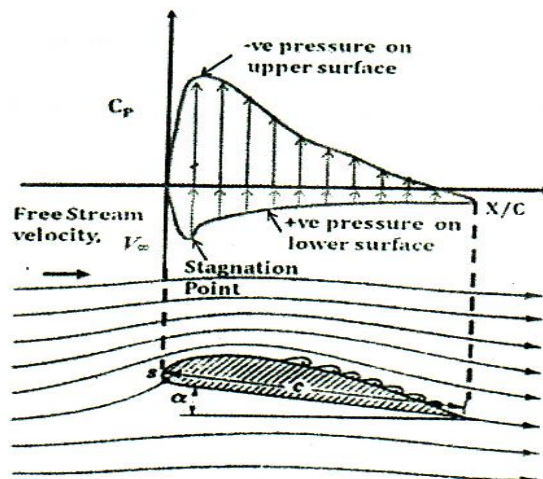


Fig.4:-Pressure Distribution over an Aero foil's Surface in terms of C_p [6,7]

$$C_{p,i} = \frac{P_i - P_{\infty}}{\frac{1}{2} \rho V_{\infty}^2} \quad (5)$$

Where, P_i is the surface static pressure at

any designated point i .

Values of C_p at any point over the airfoil surface can be approximated from the

corresponding boundary values by using the first order L arrange interpolation and extrapolation:

$$c_p(x) = \frac{(x-x_1)}{(x_0-x_1)} c_{p,0} - \frac{(x-x_0)}{(x_1-x_0)} c_{p,1} \quad (6)$$

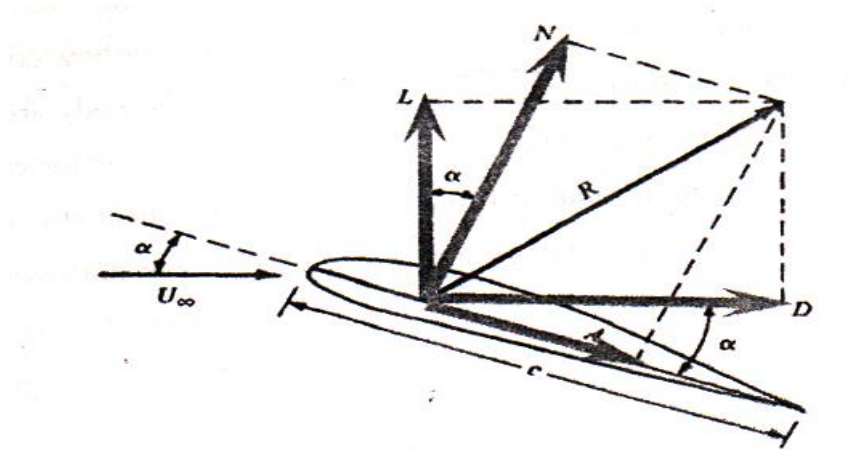


Fig.5:-Resultant Aerodynamic Force and its Components [8,9]

N = normal force = component of R perpendicular to c

A = axial force = Component of R parallel to c

The angle of attack α is defined as the angle between c and U . Hence, α is also the angle between L and N and between D and A . From Figure 5 [8,9] the following two equations can be found-

$$L = N \cos \alpha - A \sin \alpha \quad (7)$$

$$D = N \sin \alpha + A \cos \alpha \quad (8)$$

The elemental normal and axial forces acting on the elemental surface dS on the upper body surface are:

$$dN'_u = -p_u ds_u \cos \theta - r_u ds_u \sin \theta \quad (9)$$

$$dA'_u = -p_u ds_u \sin \theta + r_u ds_u \cos \theta \quad (10)$$

On the lower body surface, we have

$$dN'_l = -p_l ds_l \cos \theta - r_l ds_l \sin \theta \quad (11)$$

$$dA'_l = p_l ds_l \sin \theta + r_l ds_l \cos \theta \quad (12)$$

The total normal and axial forces per unit span are obtained by integrating Equations

In Figure 5 [8,9], by definition,

L = lift = Component of R perpendicular to U_∞

D = drag = Component of R parallel to U_∞

(9) to (12) from the leading edge (LE) to the trailing edge (TE):

$$N' = - \int_{LE}^{TE} (p_u \cos \theta + r_u \sin \theta) ds_u + \int_{LE}^{TE} (p_l \cos \theta - r_l \sin \theta) ds_l \quad (13)$$

$$A' = - \int_{LE}^{TE} (-p_u \sin \theta + r_u \cos \theta) ds_u + \int_{LE}^{TE} (p_l \sin \theta - r_l \cos \theta) ds_l \quad (14)$$

The dimensionless force coefficients are defined as follows:

Lift coefficient: $C_L = \frac{L}{q_a s} \quad (15)$

Drag coefficient: $C_D = \frac{D}{q_a s} \quad (16)$

Normal force coefficient: $C_N = \frac{N}{q_a s} \quad (17)$

Axial force coefficient: $C_A = \frac{A}{q_a s} \quad (18)$

From Figure 6 [2] the following equations can be found-

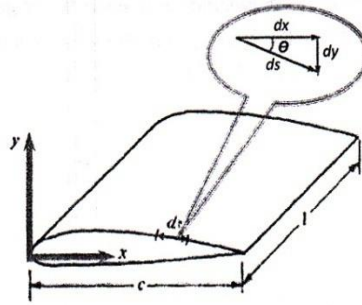


Fig.6:-Geometrical Relationship of Differential Lengths [2].

$$dx = ds \cos \theta$$

$$dy = -ds \sin \theta$$

$$S = c(1) = c$$

Substituting the above expressions of dx , dy and S into Equations (13) and (14), dividing by we obtain the following integral forms for the force and moment coefficients:

$$C_n = \frac{1}{c} \int_0^c (C_{p,l} - C_{p,u}) dx +$$

$$\frac{1}{c} \int_0^c \left(C_{f,u} \frac{dy_u}{dx} + C_{f,l} \frac{dy_l}{dx} \right) dx$$

(19)

$$C_a = \frac{1}{c} \int_0^c \left(C_{p,u} \frac{dy_u}{dx} - C_{p,l} \frac{dy_l}{dx} \right) dx +$$

$$\frac{1}{c} \int_0^c (C_{f,u} + C_{f,l}) dx \quad (20)$$

The normal and axial force acting on an airfoil section as follows:

$$C_n = \frac{1}{c} \int_0^c (C_{p,l} - C_{p,u}) dx \quad (21)$$

$$C_a = \frac{1}{c} \int_0^c \left(C_{p,u} \frac{dy_u}{dx} - C_{p,l} \frac{dy_l}{dx} \right) dx \quad (22)$$

Both the surfaces of the wing section can be divided into small panels corresponding to a total of gaps between each pressure tap location. When n is a number of panels, the equations can be converted to:

$$C_n = \sum_{i=1}^n [(C_{p,u,i} - C_{p,l,i}) \Delta \left(\frac{x_i}{c} \right)] \quad (23)$$

$$C_a = \sum_{i=1}^n \left[\left(C_{p,u,i} \frac{\Delta y_{u,i}}{\Delta x_i} - C_{p,l,i} \frac{\Delta y_{l,i}}{\Delta x_i} \right) \Delta \left(\frac{x_i}{c} \right) \right] \quad (24)$$

The interpolated and extrapolated pressure coefficients would be applied to Equation (23) and (24) in order to get the normal and axial force at a section of interest. Lift and drag coefficient can be obtained from:

$$C_l = C_n \cos \alpha + C_a \sin \alpha \quad (25)$$

$$C_d = C_n \sin \alpha + C_a \cos \alpha \quad (26)$$

The over-all value of the coefficients for the whole wing can be found out by averaging the same values of each segments of the wing along the span.

EXPERIMENTAL SETUP AND METHODOLOGY

Experimental Setup

Similar setup has been done to conduct the experiment as that of did by Nazmul et al. 2015 [8] and Ara et al. 2018 [13]. All the models will be tested at air speed of 135km/h (0.11 Mach) i.e. at Reynolds number 2.92×10^5 in the closed-circuit wind tunnel available at the turbulence laboratory, Department of Mechanical Engineering, BUET. Two counter rotating fans are used to get the desired air speed which are powered by 400V-3 ϕ -50Hz power supply. To vary the wind speed in the tunnel from 30 km/h (0.025 Mach) to 165 km/h(0.137 Mach), a speed controller is used. The dimension of the experimental space in wind tunnel is 700 mm x 700 mm. A silencer is used at the discharge to reduce the sound level. The details of the experimental setup in wind tunnel are shown in Figure 7. To performs the experiment in the open-air condition the diffuser at the end of the test section is taken out and the discharge side of the test section is fitted with a 700 mm×700 mm discharge duct. In the wind tunnel, a fixture is installed to rotate the wing modes at angle of attack from 0° to 20° with a step of 2°.

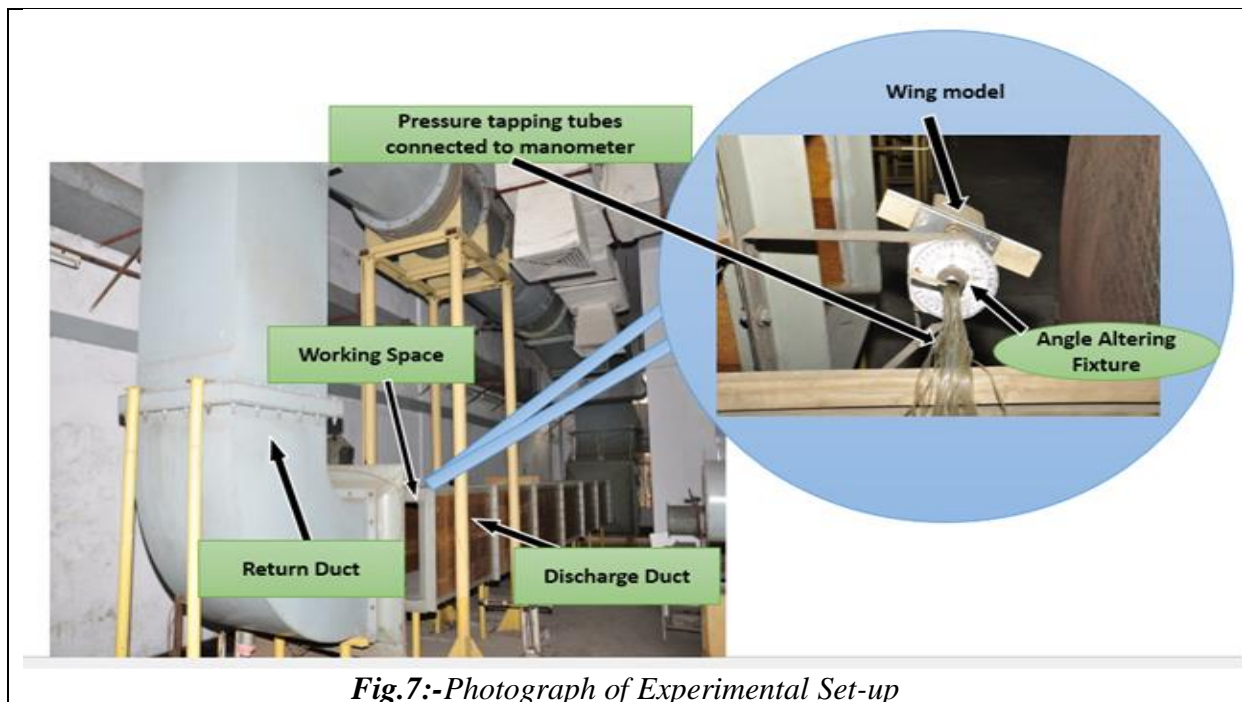


Fig.7:-Photograph of Experimental Set-up

Methodology

In this present study, we followed the methods of Nazmul et al. 2015 [8] and Ara et al. 2018 [13]. The step by step procedures are follows:

- 1) From the wind tunnel testing, the static pressure at different angles of attack ($\alpha = 0^\circ, 2^\circ, 4^\circ, 6^\circ, 8^\circ, 10^\circ, 12^\circ, 14^\circ, 16^\circ, 18^\circ$ and 20°) are measured from both upper and lower surfaces of all the wing models of different aspect ratios through different pressure tapings by using a multi-tube manometer.
- 2) The respective coefficient of pressures (C_p) of the all the wing models are calculated from the static pressure data using equation (1) to (6).
- 3) The values of C_p of both surfaces of individual models of different aspect ratios are plotted in C_p versus %C graph to observe the pressure pattern of four segments (A, B, C, D) of each model along the chord length.
- 4) From equation (23) to (26), C_L and C_D of all the wing models of different aspect ratios at every angle of attack are calculated.

- 5) Coefficient of lift to drag ratio (C_L/C_D) at different angle of attack for all the wing models are measured from the value of C_L and C_D at respective angle of attack.
- 6) The lift characteristics, drag characteristics and coefficient of lift to drag ratio (C_L/C_D) of all the wing models are analyzed and compared with each other to find the optimum wing model.

RESULTS AND DISCUSSION

The pressure coefficients of both upper and lower surfaces of different wing models for different aspect ratios are measured through the wind tunnel testing to analyze aerodynamic characteristics. The pressure coefficients are plotted along chord wise positions (% C) at different angles of attack for each of the four segments (A, B, C and D) of all the wing models. Surface pressure distribution of all the wing models are discussed and compared. The data taken from the pressure distribution are used to calculate normal and axial forces on the wing models. These normal and axial forces are used to determine coefficient of lift (C_L),

coefficient of drag (C_D) and coefficient of lift to drag ratio (C_L / C_D) of individual wing. Then the effect of angle of attack on C_L , C_D and (C_L / C_D) are studied and used in comparison. From the analysis of coefficient of lift to drag ratio (C_L / C_D) the optimum wing is found.

Surface Pressure Distributions

The pressure distributions of both upper and lower surfaces along the chord length of four segments (Segment- A, B, C and D) of three experimental wing models at 0° , 2° , 4° , 6° , 8° , 10° , 12° , 14° , 16° , 18° and 20° angle of attack (AOA) are plotted. In the figures, the horizontal axis represents the percentage of the chord length (%C) and the vertical axis represents the surface pressure coefficient (C_p). The negative pressure coefficients are shown by the vertical axis above zero line and the positive pressure coefficients are shown by

vertical axis below zero line. In all figures, C_{pu} stands for upper surface pressure coefficient and C_{pl} stands for lower surface pressure coefficient.

Figure 811 show the pressure distribution of all the wing models for four segments (A, B, C, D) at 4° angle of attack. From all the Figure, it is observed that the upper surface suction pressure is lowest for wing of AR 1 and highest for the wing of AR 2. The lower surface pressures of all the wing models remain at the positive pressure side throughout the chord length and are close to each other but highest value is obtained for wing of AR 2. As a result, the pressure difference between the upper and lower surface of the wing of AR 2 is highest. For all the wing models of different aspect ratios the upper surface pressure increases gradually from leading edge to trailing edge and lower surface pressure decreases.

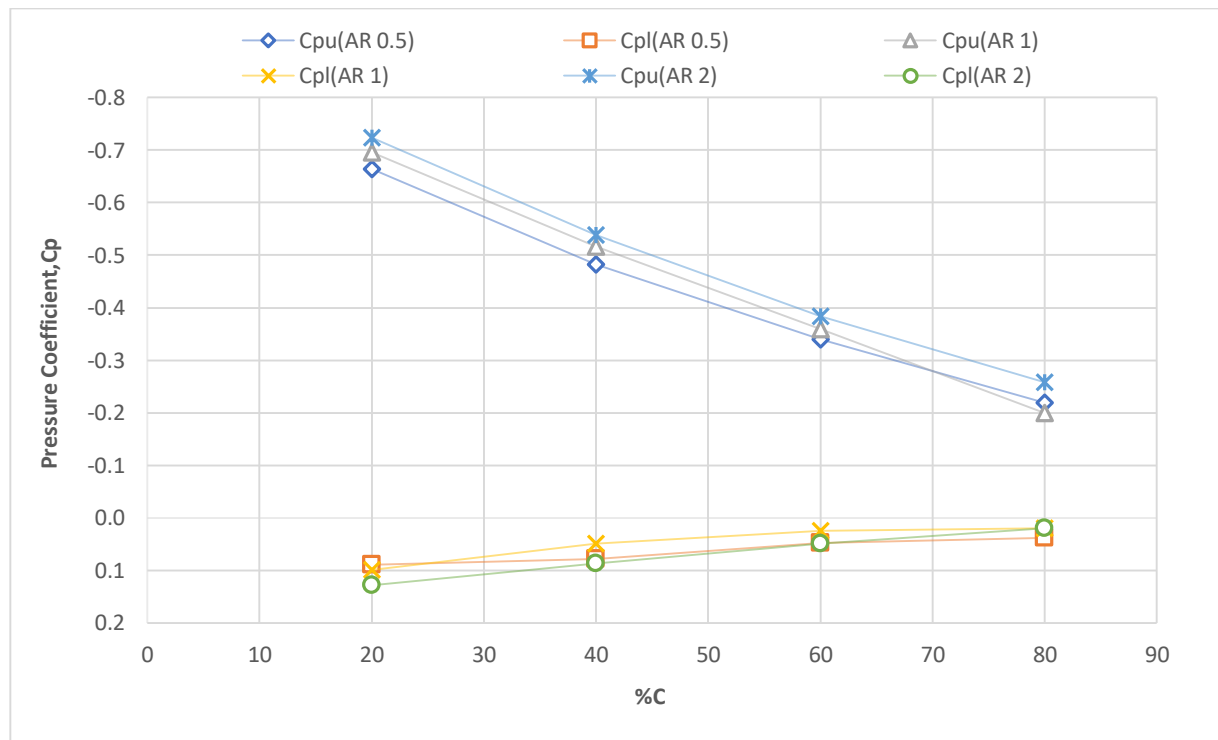


Fig.8:-Pressure coefficient (C_p) distribution of segment A at 4° AOA

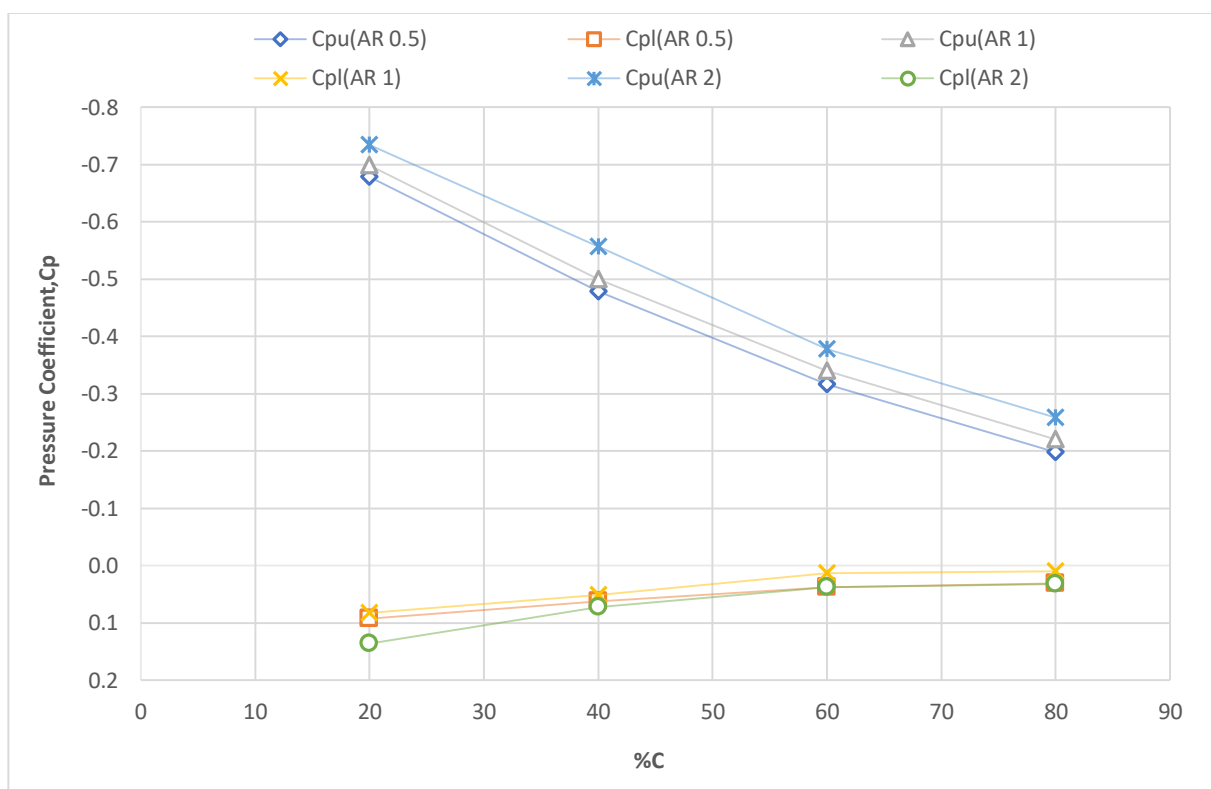


Fig.9:- Pressure coefficient (C_p) distribution of segment B at 4° AOA

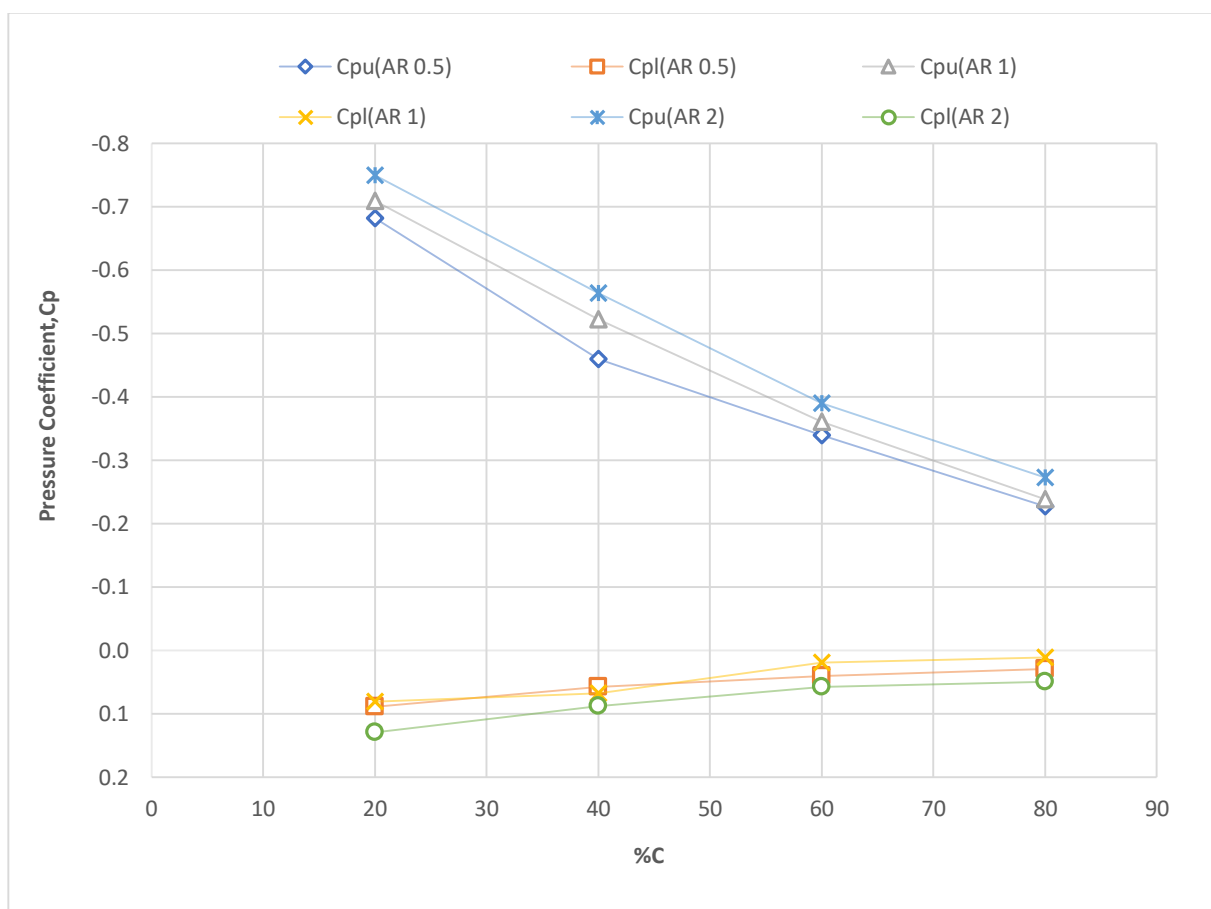


Fig.10:- Pressure coefficient (C_p) distribution of segment C at 4° AOA

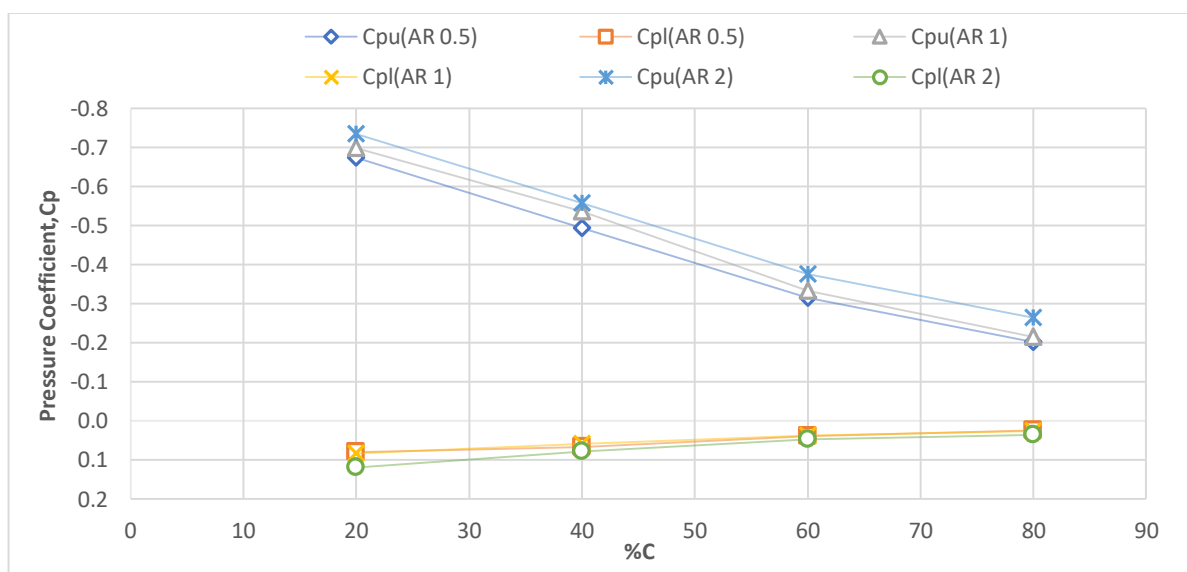


Fig.11:-Pressure coefficient (C_p) distribution of segment D at 4° AOA

The surface pressure distributions of all the wing models at 10° angle of attack are shown in Figure 12-15 for four segments (A, B, C, D). From the figures, it is observed that upper surfaces of all wing models are having higher negative pressure than the lower surface pressure of the respective wing models. For the wing models of AR 1 and AR 0.5, the lower surface pressure decreases slowly from 20% C to 80% C. The upper surface pressure increases gradually from leading

edge to trailing edge. For wing of AR 2 as well, upper surface pressure increases and lower surface pressure decreases from leading edge to the trailing edge. But the upper surface pressure is lowest for wing of AR 0.5 and lower surface pressure is highest for wing of AR 1. As a consequence, the difference between upper and lower surface pressure is observed maximum for wing of AR 2 and the highest difference is achieved at 20% C.

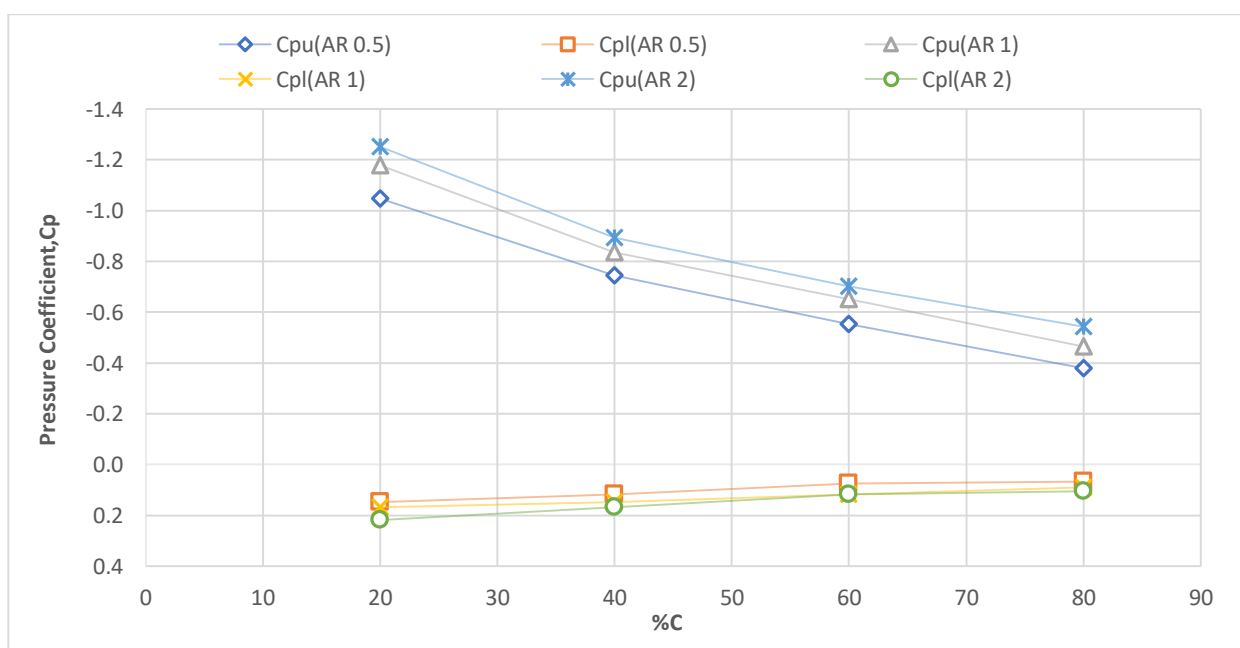


Fig.12:-Pressure coefficient (C_p) distribution of segment A at 10° AOA

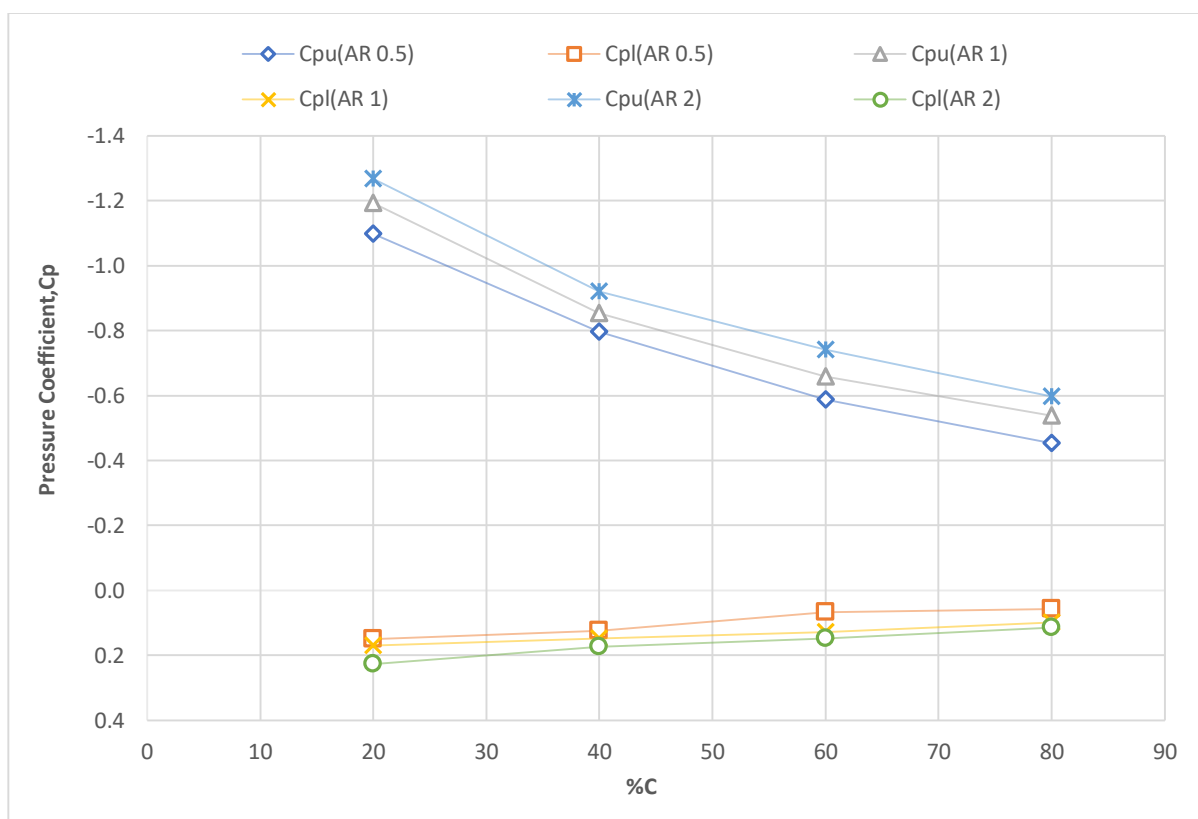


Fig.13:-Pressure coefficient (C_p) distribution of segment B at 10° AOA

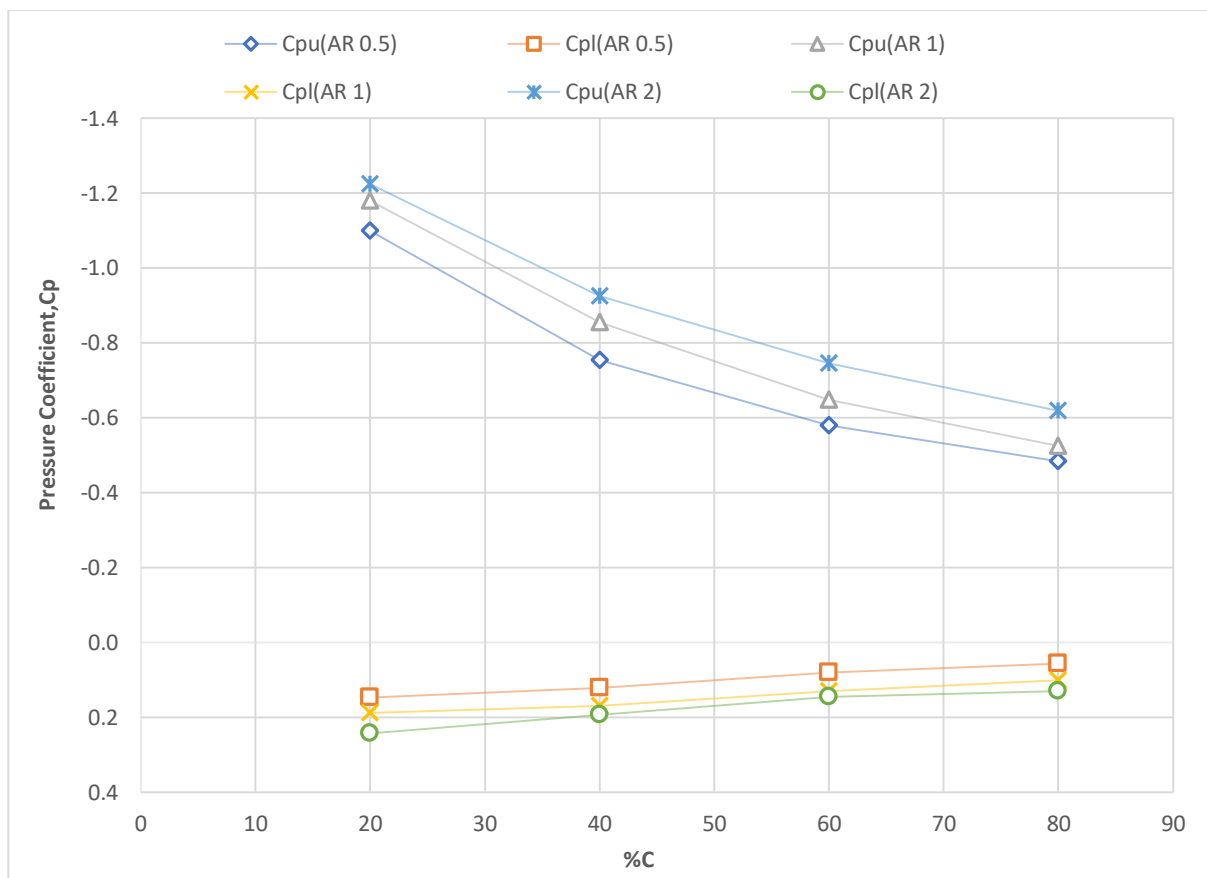


Fig.14:-Pressure coefficient (C_p) distribution of segment C at 10° AOA

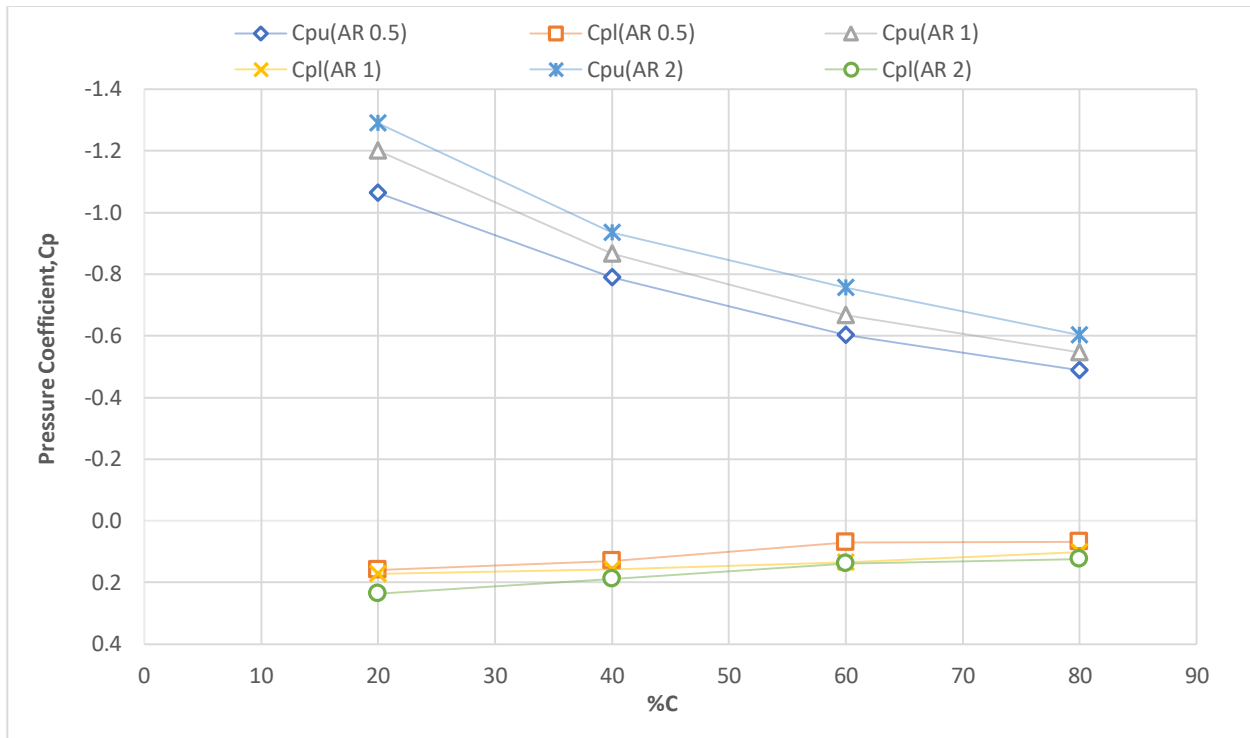


Fig.15:-Pressure coefficient (C_p) distribution of segment D at 10° AOA

All the pressure distribution curve at different angle of attacks also shows the similar pattern. In comparison to the pressure difference of the surfaces of model of AR 2 is higher than model of AR 1 and model of AR 0.5. Another observation from the figures is that the lower surface pressure of all the wing models for all the segments are higher than all the previous angle of attack. The highest-pressure difference between the upper and lower surfaces is obtained for wing models of AR 2 and it is lowest for wing models of AR 0.5. For all the segments the lower surface pressure decreases from 20%C to 80%C and upper surface pressure increases from leading edge to trailing edge.

Lift Characteristics

The lift characteristics of wing models at different angles are shown in Figure 16. The figure shows that as the angle of attack increases, the lift also increases peaking a maximum value at a certain AOA. After this maximum value of angle of attack, lift decreases drastically due to

flow separation over the aero foil surface. From the figure, it is seen that the lift coefficient curve goes up from 0° angle of attack up to 12° angle of attack for all the wing models and then drops suddenly after 12° angle of attack. Thus, the critical angle of attack of all wing models is around 12° beyond which the stall happens. The angle at which stall occurs is called stalling angle of attack beyond which flow separation occurs. It is seen from the figure that for all wing models stall occurs at approximately 12° angle of attack. Among the three wing models wing of AR 2 has the higher lift coefficient than other two wing models of AR 1 and AR 0.5. The ratio between the lift coefficient and the angle of attack is maximum at 12° angle of attack for all the wing models and for this reason this AOA is the optimum AOA which indicates that to get highest lift from NACA 0012 wing, it must be placed at around 12° to the path of flight. This analysis has analogous nature to Kopac analysis [11] and National Aero foil Data NACA 0012 [4].

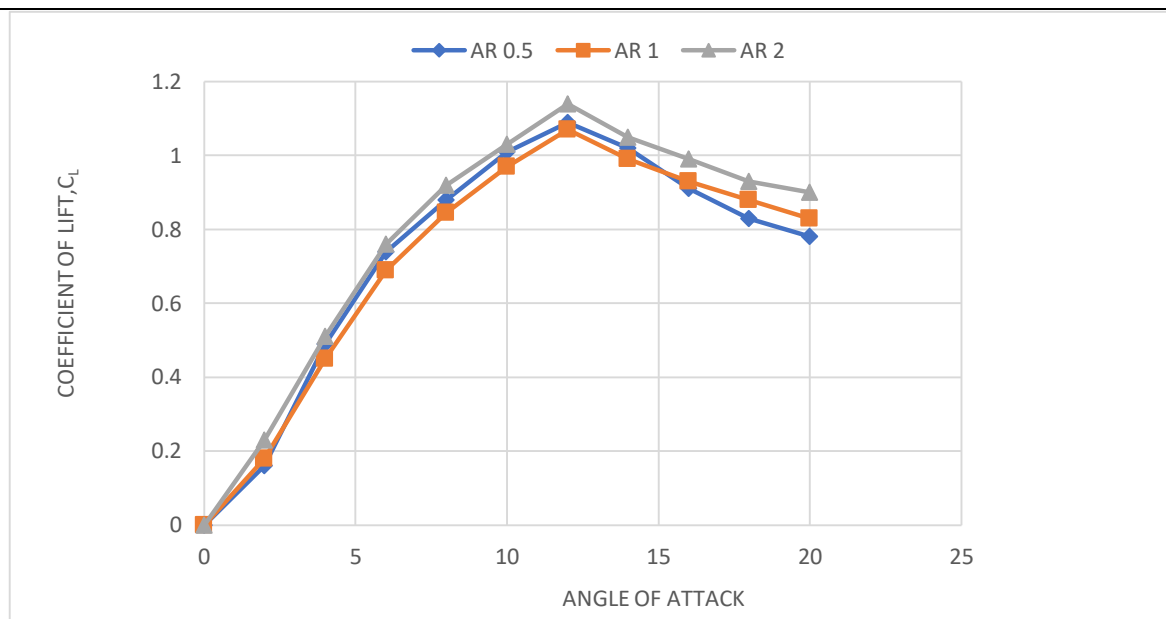


Fig.16:- Coefficient of lift vs angle of attack

Drag Characteristics

Figure 17 illustrates the drag coefficients of the wing models under test for different angle of attack. Graph shows that drag coefficient is higher for wing model of AR 0.5 than other two models and it is lower for wing model of AR 2. Initially, the rate of increment of drag is slower for angle of attack ranging from 0° to 8° . After that a noticeable increase of drag coefficient is seen from 8° to 20° angle of attack. It is also seen from the figure that drag

coefficient increases dramatically after the stalling angle of attack. This is due to the fact that air detaches from the surface of the airfoil because of adverse pressure gradient after stalling angle of attack. It signifies that if the AOA further increases, then drag will dominate the lift and as a result stall will occur. Present experimental results show similar nature as of Kopac analysis [11] and National Aerofoil Data NACA 0012 [4].

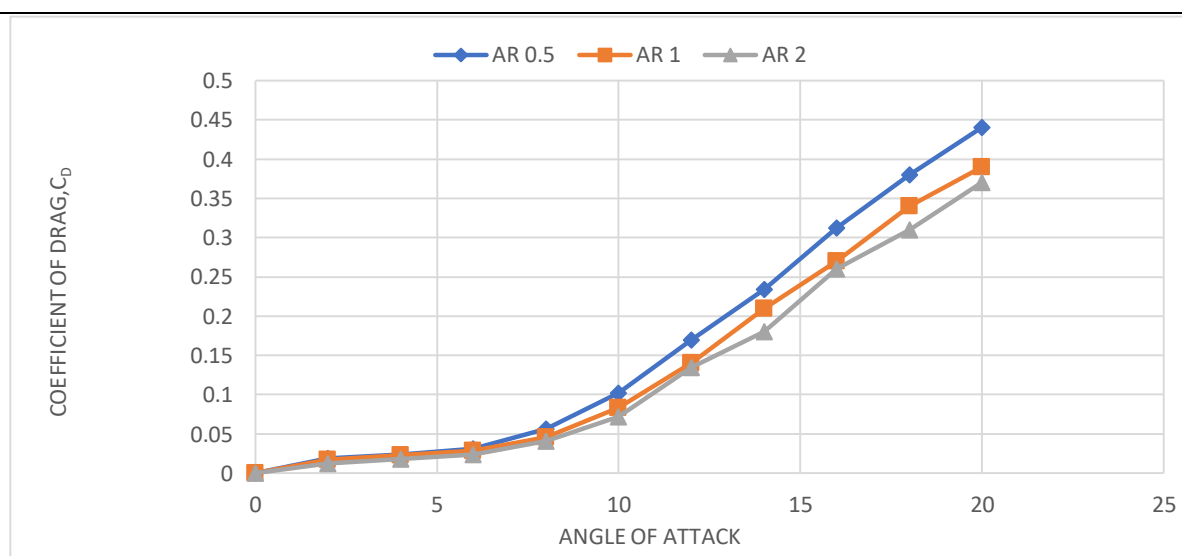


Fig.17:- Coefficient of Drag vs angle of attack

Lift Coefficient to Drag Coefficient Ratio

Figure 18 shows the values of lift coefficient to drag coefficient ratio which are plotted for various angle of attack. From the figure it is observed that wing model of AR 2 has the highest lift coefficient to drag coefficient ratio, while the AR 0.5 has the lowest lift to drag coefficient ratio compared to another wing model. For the wing model of AR 2, the lift to drag ratio increases rapidly reaching

a peak value of 31.67 at 6° AOA. Other two models also experience similar trend but the values are lower than wing model of AR 2. It is also seen from the figure that in the interval 6° to 12° AOA, there is a significant decrease of lift to drag coefficient ratios. After 12° AOA, the ratios decrease gradually for all the wing models. The present experimental results yield that among the three wing models the wing model of AR 2 is the most efficient.

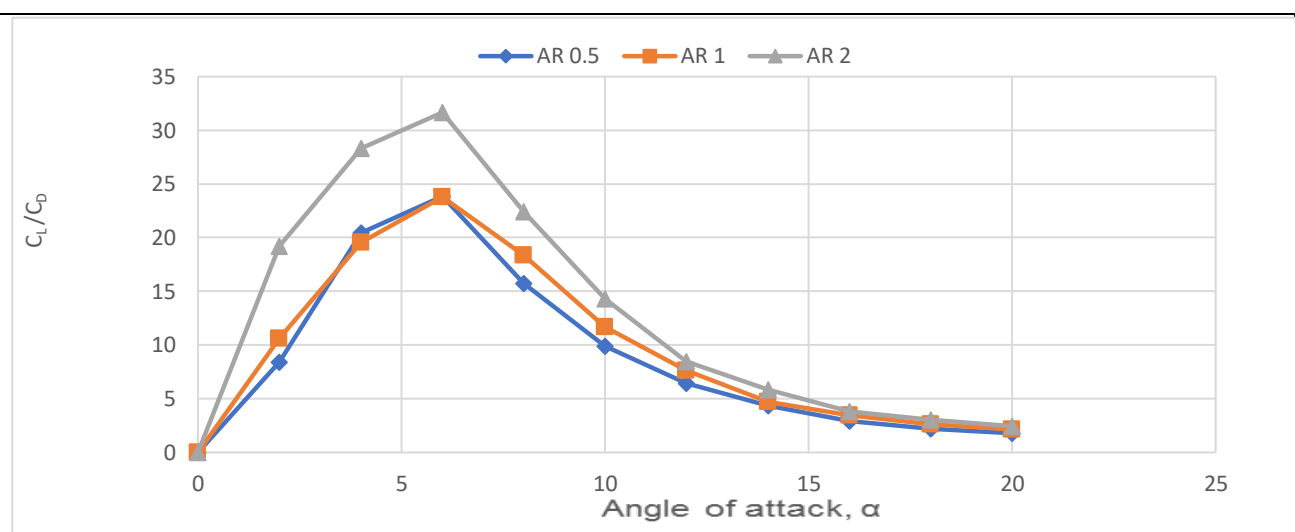


Fig.18:-Comparison of Lift Coefficient to Drag Coefficient curve for different aspect ratios

CONCLUSIONS

The current experiment has been done to show a relative study among three different aspect ratios of AR 2, AR 1 and AR 0.5 of NACA 0012 wing. It is seen that, for the wing model of AR 2, the difference between upper and lower surface pressure is relatively greater than that of other wing models. This is because for identical wing area the wing model of higher aspect ratio decreases the strength of vortices at the wingtip by decreasing the vortex produced at the tip more successfully than other wing models. From the figure of lift coefficient versus angle of attack, it is seen that for all wing models of different aspect ratios stalling angle of attack remains at 12° and the stall occurs after this angle of attack. It also observed

from the drag coefficient graph that for AR 2, drag coefficient is lowest. Moreover, the wing model of AR 2 has the largest value of lift to drag coefficient ratio than other two wing models. So, after analyzing the comparative study it is found that wing model of AR 2 is the optimum wing model.

REFERENCES

1. Makwana, P. B., & Makadiya, J. J. (2014). Numerical Simulation of Flow Over Airfoil and Different Techniques to Reduce Flow Separation Along with Basic CFD Model: A Review Study. *International Journal of Engineering Research*, 3(4).

2. Anderson Jr, J. D. (2010). *Fundamentals of aerodynamics*. Tata McGraw-Hill Education.
3. Eppler, R. (2012). *Airfoil design and data*. Springer Science & Business Media.
4. National Aerofoil Data NACA 0012, Online data, <http://airfoiltools.com/airfoil/details?airfoil=naca0012-il>.
5. Abbott, I. H., & Von Doenhoff, A. E. (2012). *Theory of wing sections: including a summary of airfoil data*. Courier Corporation.
6. Martinat, G., Braza, M., Hoarau, Y., & Harran, G. (2008). Turbulence modelling of the flow past a pitching NACA0012 airfoil at 105 and 106 Reynolds numbers. *Journal of Fluids and Structures*, 24(8), 1294-1303.
7. Aşkan, A., & Tangöz, S. (2018). The impact of aspect ratio on aerodynamic performance and flow separation behavior of a model wing composed from different profiles. *Journal of Energy Systems*, 2(4), 224-237.
8. Haque, M. N., Ali, M., & Ara, I. (2015). Experimental investigation on the performance of NACA 4412 aerofoil with curved leading edge planform. *Procedia Engineering*, 105, 232-240.
9. Alam, G. M. J. (2011). Interference Effect and Flow Pattern of Four Biplane Configurations using NACA 0024 Profile. In *Proceedings of The International Conference on Mechanical Engineering, Dhaka Bangladesh*.
10. Mizoguchi, M., & Itoh, H. (2013). Effect of aspect ratio on aerodynamic characteristics at low Reynolds numbers. *AIAA journal*, 51(7), 1631-1639.
11. Kopac, M., Yilmaz, M., & Gultop, T. (2005). An investigation of the effect of aspect ratio on the airfoil performance. *Am J Appl Sci*, 2(2), 545-549.
12. Shehata, A. S., Xiao, Q., Saqr, K. M., Naguib, A., & Alexander, D. (2017). Passive flow control for aerodynamic performance enhancement of airfoil with its application in Wells turbine—under oscillating flow condition. *Ocean Engineering*, 136, 31-53.
13. Ara, I. (2018). Experimental study on the aerodynamic performance of winglets with curve edged wing of NACA 4412.
14. Patel, K. S., Patel, S. B., Patel, U. B., & Ahuja, A. P. (2014). CFD Analysis of an Aerofoil. *International Journal of Engineering Research*, 3(3), 154-158.
15. Kevadiya, M. (2013). CFD analysis of pressure coefficient for NACA 4412. *International Journal of Engineering Trends and Technology, Chennai*, 4(5), 2041-2043.